Proceedings of the ASME 2018 37th International Conference on Ocean, Offshore and Arctic Engineering
OMAE2018
June 17-22, 2018, Madrid, Spain

OMAE2018-77464

NUMERICAL STUDY OF A FISHING VESSEL OPERATING IN PARTIALLY ICE COVERED WATERS

Karl Gunnar Aarsæther
SINTEF Ocean
Tromsø, Norway

Biao Su
SINTEF Ocean
Trondheim, Norway

David Kristiansen
SINTEF Ocean
Trondheim, Norway

ABSTRACT

The Arctic ocean has been the focus of increasing activities in oil and gas, marine traffic and fisheries as the resources in the Arctic area becomes more attractive for exploitation. There have been several studies on the response of ships and structures in ice covered waters, mainly for oil and gas applications. This paper presents a scenario simulation model for fisheries, crab pot retrieval, in partially ice covered waters. Snow crab fisheries in the Barents Sea is an ongoing commercial activity where partial ice covers may drift over crab pots which need retrieval. This scenario is unique in the sense that the ship and ice can be expected to experience wave forcing in addition to the ice–structure interaction. The complexity of such scenarios favor simplified models and a coupled simulation model consisting of ship hydrodynamics, ice hydrodynamics, ice–ice and ice–ship interactions. A case vessel is presented together with a scenario simulation model which is used to assess the ice impact forces during operations and the amount of ice interaction which can be expected in the region where the pot string is retrieved from the ocean.

INTRODUCTION

The Arctic oceans have become an area of importance for several nations as technology allows the exploitation of the natural resources in the region. Marine operations in the Arctic is associated with remoteness, rapidly changing conditions and the presence of ice and snow both on land and on the oceans. The Arctic oceans have recently been the focus on research and development for offshore oil & gas exploitation and seaborne transport as the region contains undeveloped hydro-carbon resources and the receding ice cover has promised to make the northeastern sea route between Europe and Asia navigable in larger parts of the year.

The Barents Sea is at the same time one of the most productive areas of marine biomass and exploitation of its seafood resources has long been an important part of the economies of the northern regions of Europe. The warming climate which has made more of the Artic oceans available has also lead to the migration of fish stocks to the north and east [1]. The migration of fish into the Arctic ocean and increased exploitation of existing Arctic species such as king crab and snow crab has added fisheries to the list of marine operations in the Arctic oceans. The patterns of fisheries are dictated by the migration pattern of their target species, which may pull the fisheries fleet close to the ice edge. Fishing vessels that find themselves operating close to the ice edge may encounter regions of broken ice fields due to the shifting nature of the ice edge. This is a particular issue for operation of stationary fishing gears such as crab pots where ice may move over already deployed gear and leave the fishermen with the option of operating in ice, or risk losing the gear due to ice damage.

A numerical simulation model for ice–ice and ice–structure interactions has been developed and compared with experimental and field measurement data [2,3]. A model for the fishing vessel and gear are used in this paper to study the ice impact forces, resulting motions and ice buildup of a vessel operating in partially ice covered waters. The ice impact forces are calculated based on a viscoelastic-plastic rheological model [4]. The 6 degrees-of-freedom (DOF) rigid body motions of the vessel are simulated by considering its interactions with a number of broken ice pieces driven by waves. The ice buildup on the hauling side of the fishing vessel is tracked and its effect on the hauling operations is evaluated. This paper, in general,

presents a unique scenario simulation and relevant results that can be used for analyses of fisheries operations in ice.

Studies of hydrodynamic interaction between broken ice pieces has been conducted in [5,6], and the application of simplified rigid body models for calculating broken ice field dynamics has been presented in [7,8]. The rigid body models for a broken ice floe field is computationally effective and produce good agreement with experiments. The rigid body dynamic formulation of a broken ice field was considered a good candidate for implementation of ship-ice interaction in the presence of waves. This paper shows the use of simplified models for ice hydrodynamics in was with hydrodynamics for vessels in waves.

MATERIALS AND METHODS

This paper presents numerical simulations of ice accretion and impact forces of a crab fishing vessel operating in broken ice with the presence of waves. The dynamics and hydrodynamics of the fishing vessel and ice in waves is modelled and the surface region where the crab pots are retrieved are found by application of a numeric simulation model for the fishing gear. The simulation model for ice-ice and ice-structure interaction and hydrodynamics presented in [2,3] is combined with a time domain simulation model of a vessel and a model for a string of crab pots based on [9]. The numerical simulation model was implemented in FhSim [10] which was used to make a scenario simulation model used for systematic variations of parameters.

FISHERIES VESSEL

A hull form is the first step in evaluating the effect of ice, current and waves. The hull form is needed in order to generate a dynamic vessel model which can respond to waves and interact with the ice floes and simulate retrieval of gear. The vessels engaged in snow crab fisheries from Norway are repurposed vessels due to the recent development of the fisheries. The vessels are of medium size and with older hull forms, often without bulbous bows which are common on ocean going fisheries vessels. The main dimensions and year of build of vessels engaged in crab fisheries in the Barents sea is seen in table 1.

Vessel	*Length*	*Breadth*	*Build year*
Arctic Pioneer	44.9m	8.5m	1967
Northeastern	51.6m	8.5m	1970
Prowess	60.2m	11m	1988

Table 1. Main particulars and build year for three vessels engaged in snow crab fisheries in the northern Barents Sea.

A vessel hull form was modelled for use in simulations to represent the currently used vessels without bulbous bows. The main particulars of the case vessel are given in Tab. 2. The body plan of the vessel in seen in Fig. 2 with sections in 3m increments from -3 m aft of AP to 60m. The figure show 21 sections with a common midship section.

Length	*63m*
Breadth	11.2m
Draught	3.8m
Displacement	1700 tons

Table 2. Main particulars for case vessel

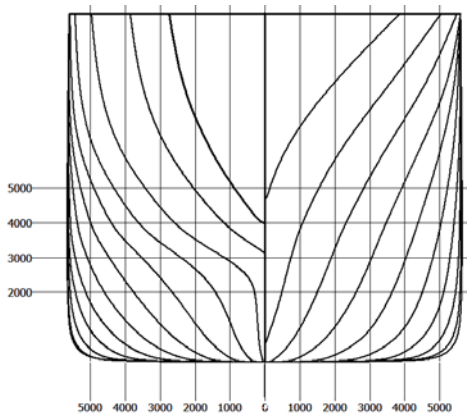

Figure 1. Section plan for case vessel with similar characteristics as Norwegian snow crab fisheries vessels. Numbers in figure show offset in mm from baseline and center line.

DYNAMIC VESSEL MODEL

The dynamic response of vessels in waves can be predicted with potential theory programs operating in the frequency domain. However, the results from the potential theory is difficult to extent into a simulation of a vessel operating in ice as the interaction forces between the vessel and the ice influence both vessel and ice motions. The added mass, damping and wave excitation force of the fisheries vessel was calculated by application of the 2D potential theory code VERES [11]. The potential theory coefficients in the frequency domain was then transformed to the time domain by a linear system approximation of the convolution integral of Cummin's equation [12] as proposed in [13]. This results in an equation system on the form shown in Eq. 1. The excitation forces F_{wave} are the wave-to-force RAOs derived from potential theory while F_{ext} are external forces from connected models.

$$\sum_{j=1}^{6}(M_{ij} - A_{\infty,ij})\ddot{x}_j + B_{ij}\dot{x}_j + \mu_{ij} + C_{ij}x_j = F_{wave,i} + F_{ext,i}, i = 1..6 \quad (1)$$

Where μ_{ij} is the output of a LTI companion system which approximate the added mass and damping derived from potential theory, details can be found in [13 ,14]. External forces can be applied to the right side of the equation in addition to the wave excitation force. In this paper the important external force is the ship-ice interaction force which can be calculated and included in this equation system to make the potential theory results interact with an broken ice field model with individual floe dynamics.

CONTACT DETECTION AND ICE FORCE CALCULATION

In the simulation of ice–ice and ice–structure interactions, determining the contact surfaces between interacting ice floes and structures at each time step is a critically important and time-consuming calculation. An efficient 3D contact detection algorithm, called the fast common-plane (FCP) method [15], was used in the present numerical model. Herein, a common plane (CP) is a plane that, in some sense, bisects the space between the two contacting particles [16]. As a result of using CP, the expensive particle-to-particle contact detection problem reduces to a much faster plane-to-particle contact detection problem. Once the CP is established between two particles, the normal to the CP defines the direction of the contact normal, which in turn defines the direction of the normal contact force between the two particles. As compared with the conventional CP algorithms, the FCP approach recognizes that a common plane has identifying characteristics, which dramatically reduce the search space for the common plane. A thorough description of the FCP approach can be found in [16].

When a CP is found and the two ice floes are intersecting (see e.g. Fig. 2), the depth of overlap (δ_c) and the intersection area (A_c) can be determined by solving a simple segment–plane interaction problem described in [2]. Multiple contacts are allowed in the simulation of ice–ice and ice–structure interactions and a viscoelastic-plastic rheology (see e.g. Fig. 3 and details can be found in [4]) is applied at all contacts. Hence the normal contact force at time step p, $F_n^c(t_p)$, is expressed as:

$$F_n^c(t_p) = k_{ns}\delta_c - k_{nv}v_n \tag{2}$$

where k_{ns} is the normal elastic stiffness; k_{nv} is the normal viscous damping coefficient; v_n is the relative velocity (between the two contacting objects) in the normal direction. The magnitude of the normal contact force is controlled by a plastic limit expressed as:

$$\left|F_n^c(t_p)\right| \le \sigma_c A_c \tag{3}$$

where σ_c is taken to be the uniaxial compressive strength of ice. The tangential contact force at time step p, $F_t^c(t_p)$, is expressed as:

$$F_t^c(t_p) = F_t^c(t_{p-1}) - k_{ts}v_t\Delta t \tag{4}$$

where $F_t^c(t_p)$ is the tangential contact force at time step $p-1$; k_{ts} is the tangential elastic stiffness; v_t is the relative velocity in the tangential direction; Δt is the time step. The magnitude of the tangential contact force is controlled the Coulomb limit expressed as:

$$\left|F_t^c(t_p)\right| \le \mu\left|F_n^c(t_p)\right| \tag{5}$$

where μ is the frictional coefficient.

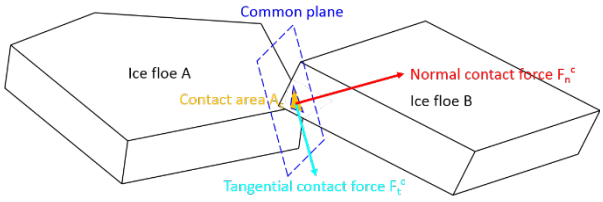

Figure 2. Illustration of the common plane and the normal and tangential contact forces between two interacting ice floes

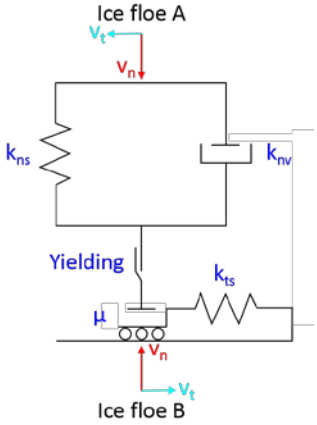

Figure 3. Illustration of the ice–ice (and ice–structure) interaction force model [14]

Kinematics of the Ice Floe

The dynamic responses of the ice floe in current and wave were obtained from the solution of the 6×6 linear system, derived by applying Newton's second law in the body-fixed frame:

$$\sum_{j=1}^{6}\left[(M_{ij}+A_{ij})\ddot{r}_j + B_{ij}\dot{r}_j + C_{ij}r_j\right] = F_i, \quad i = 1,\ldots,6 \tag{6}$$

where M_{ij} are the components of the generalized mass matrix; A_{ij}, B_{ij} and C_{ij} are the 6×6 added-mass, damping and restoring coefficients, respectively; F_i are the components of the excitation forces.

The added mass and damping coefficients of the ice floes and the structure were calculated by WAMIT [14] in the frequency domain. The present numerical model requires a time-domain formulation of the frequency-dependent hydrodynamic coefficients. The added mass and damping forces from frequency-domain WAMIT data were transferred to the time

domain as with the vessel model by application of a linear system adaptation described above.

The excitation forces on a relatively small body in wave (the characteristic cross-sectional dimension of the ice floe and the structure is smaller than 1/5 of the wavelength considered in the present study) can be written as [17]:

$$F_i^p = -\iint_S p n_i ds + \sum_{j=1}^{3} A_{ij} a_{ij}, \quad i = 1,2,3 \tag{7}$$

where p is the pressure in the undisturbed wave field and $\mathbf{n} = (n_1, n_2, n_3)$ is the unit vector of normal to the body defined to be positive into the fluid. The integration is over the wetted surface of the body. Further, a_1, a_2 and a_3 are the acceleration components along the x-, y- and z-axes of the undisturbed wave field and are to be evaluated at the geometrical mass center of the body.

The first term in Equation (6) is the Froude-Kriloff force. The second term physically represents the fact that the undisturbed pressure field is changed due to the presence of the body (diffraction force), in which an approximate method is applied by using the velocity potentials due to forced motion of the body (added mass and damping) instead of the diffraction potential, for details see [17] and [18].

In addition to the Froude-Kriloff and diffraction forces, the viscous drag force is calculated using Morison's equation:

$$\mathbf{F}^v = \frac{1}{2}\rho C_d A_d |\mathbf{V}_w - \mathbf{V}_i|(\mathbf{V}_w - \mathbf{V}_i) \tag{8}$$

where ρ is the water density; C_d is the drag coefficient (≈ 1.0); A_d is a reference area (e.g. the cross-sectional area of the body perpendicular to the flow direction); $\mathbf{V}_w$ is the wave-induced particle velocity; $\mathbf{V}_i$ is the velocity of the ice floe.

Furthermore, the Coriolis effect is taken into account when solving the 6-DOF equations of motions in the body-fixed frame. Therefore the expression for the force components in Equation (5) can be written as:

$$\mathbf{F} = \mathbf{F}^p + \mathbf{F}^v + \mathbf{F}^{Cor} + \mathbf{F}^c \tag{9}$$

where $\mathbf{F} = (F_1, F_2, F_3, F_4, F_5, F_6)$ is the total external force acting on the ice floe; $\mathbf{F}^p$ is the Froude-Kriloff and diffraction forces; $\mathbf{F}^v$ is the viscous drag force; $\mathbf{F}^{Cor}$ is the Coriolis force which is a fictitious force induced by a non-uniformly rotating frame (i.e. the body-fixed frame) relative to the inertial frame (for details see e.g. [19]); $\mathbf{F}^c$ is the ice–ice and ice–structure interaction force.

SIMULATION SETUP AND PARAMETER VARIATION

The dynamic vessel model and the ice interaction model was combined into a scenario simulation model in order to carry out systematic parameter variations. The scenario was configured to mimic a snow crab fisheries vessel which is retrieving a string of pots on the starboard side and encountering a broken ice field along the path of the pot string. The ice floes may interfere with the retrieval operation on the starboard side of the vessel and two regions capable of detecting ice floes while traveling with the vessel was defined: A region covering the starboard side to detect possible interference and a smaller region to detect critical interference. An overview of the simulation scenario is seen in Fig. 4

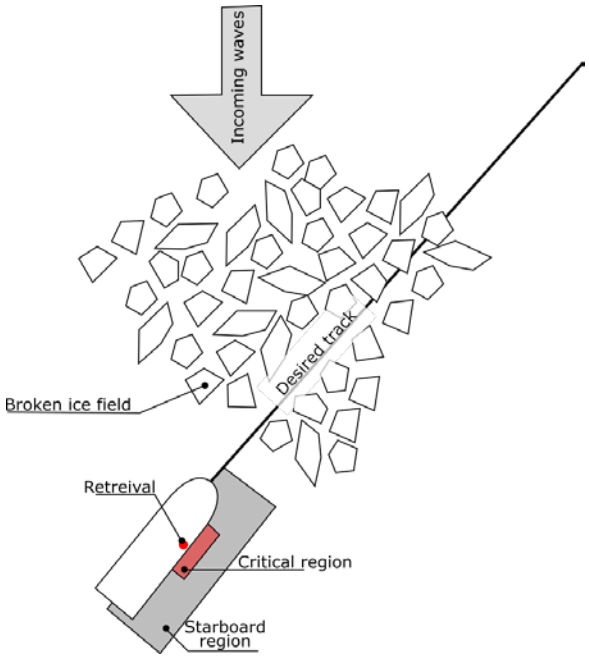

Figure 4. Illustration of simulation model with vessel, desired track along the crab pot string and detection regions on the starboard side.

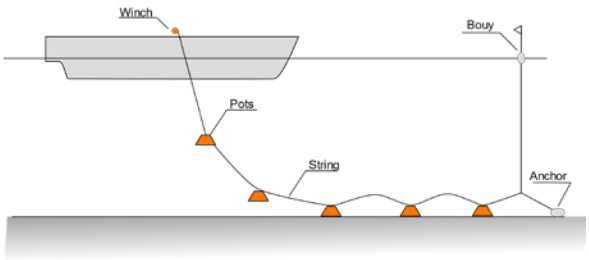

Figure 5. Schematic illustration of retrieval of a crab pot string.

The region of possible interference vas defined as covering the length of the ship and 20m starboard from the centerline of the hull. The critical interference region was defined by simulation the retrieval operation without ice present as seen in Fig. 5. The vessel was equipped with a pot string model based on the cable model used in [9]. The pot string was retrieved while the vessel was travelling at 1.5m/s. while the intersection of the pot string with the still water surface was calculated and used to define the critical region for simulations with ice present.

The vessel was navigated with simple PI control algorithms for surge force & yaw torque and waypoint navigation. The output of the PI controllers was applied directly to the vessel, but the vessel maintained its dynamic nature and experience velocity reductions from ice impacts and wave forces.

SYSTEMATIC PARAMETER VARIATIONS

The ice concentration, floe size, vessel forward speed and significant wave height was varied systematically as shown in Tab. 3 which resulted in 72 simulation cases. The ice floe sizes and thickness were varied uniformly by 20% around the given floe size. The ice floe fields were preprocessed and used as input to the simulation. The ice floe field was 300m x 300m for the 10m cases and 600m x 600m for the 20m cases.

Parameter	*Value*
Ice Concentration	30%, 50%, 70%
Significant wave height	2m, 3m, 4m
Vessel forward speed	1 m/s, 1.5m/s, 2.0m/s, 2.5m/s
Floe size / thickness	10m/0.5m, 20m/1m
Number of variations	**72**

Table 3. Parameter variations for numeric simulations.

The vessel was travelling towards the ice floe field with an angle of 28 degrees towards the incoming waves and ice floes. A screenshot at the start of the scenario is seen in Fig. 8. Waves were generated from a JONSWAP spectrum with mean wave period of 11 seconds.

RESULTS

The results from the scenario simulations are presented below starting with determining the extents of the critical interaction region and continuing with ice impact forces and amount of ice floe interaction. Detailed time series from the simulations were kept, but only aggregated results are shown below due to space considerations.

CRITICAL ICE REGION

The critical interaction region was determined from a single simulation. The crab pot string model was a discrete cable model with a heavier and shorter cable section representing pots. The cable was retracted into an endpoint representing a winch placed 7.2m above the surface 8m from the vessels centerline. The intersection between the gear and still water surface was found from the direction of the tension vector at the end of the gear. It was observed that there were fluctuations in the position of the intersection point as the pot string model was retracted and elements disappeared at the retraction end. The distribution of the longitudinal and transverse intersection coordinates relative to the winch point is seen in Fig. 6.

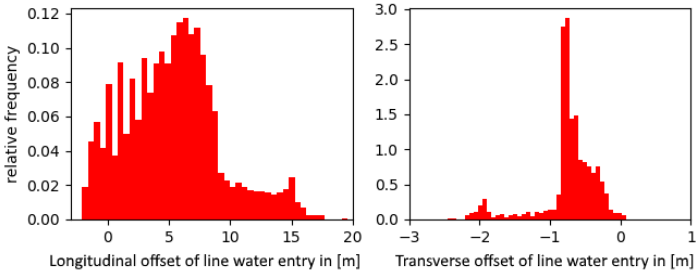

Figure 6. Relative frequency of water entry point relative to crane tip for retrieval of crab pot linel.

Positive values for the longitudinal direction is towards the bow and positive transverse direction is towards starboard (away from vessel). The geometry of the gear and vessel is seen in Fig. 7. The violet line is the crab pot string and the red line is the desired course track mirroring the crab pot string on the surface.

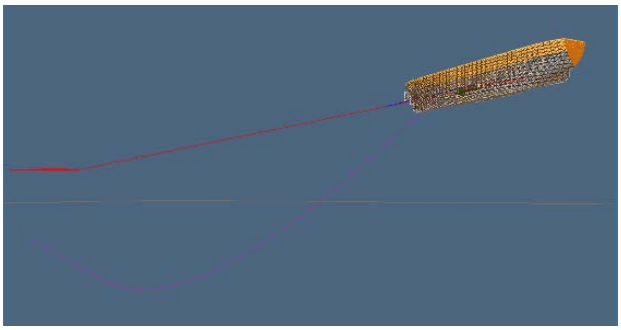

Figure 7. Illustration of simulation model with vessel, and retrieval of crab pot string.

The extent of the critical region was determined to be 20m in the longitudinal direction and 8m in the transverse direction.

ICE IMPACT FORCES AND ACCRETION

The simulations for parameter variations was conducted on a standard laptop computer with an Intel Core i7 CPU and 16gb RAM. The complete parameter sweep was completed within 16 hours. The results of each simulation run was a collection of time series for variables such as ship speed, instantaneous ice-ship impact force and detected ice floes in the starboard & critical regions travelling with the vessel. The time series were truncated to cover only the time from the first ice floe entered the starboard detection region to the point where the last ice floe left the starboard detection zone. A screenshot of the start of a parameter variation simulation is seen in Fig. 8.

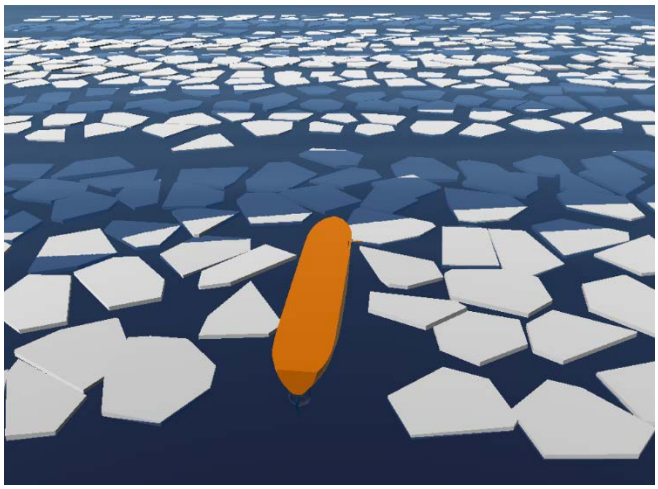

Figure 8. Illustration of simulation model with vessel, vessel contact geometry and ice floe field. 10m ice floes.

ACCRETION

Ice floes in the starboard and critical region showed little variation with the parameters ship forward speed and significant wave height. There were variations when considering floe size and ice concentration. The median number of floes in the two regions are shown in Fig 9.

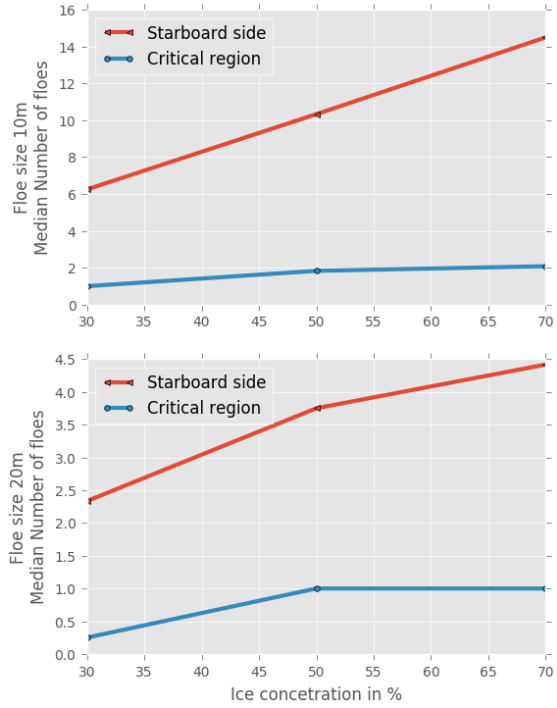

Figure 9. Median number of ice floes in the starboard and critical regions for 10m and 20m ice floe size and 30%, 50% and 70% ice concentration.

IMPACT FORCES

The time series of the ice-vessel impact forces were fluctuating due to varying blockages and piling of ice floes and the peak values of the absolute value of the 3D force was extracted. The peak values were sorted and the mean of the largest 30% of peak values, significant force, are shown in Fig. 10.

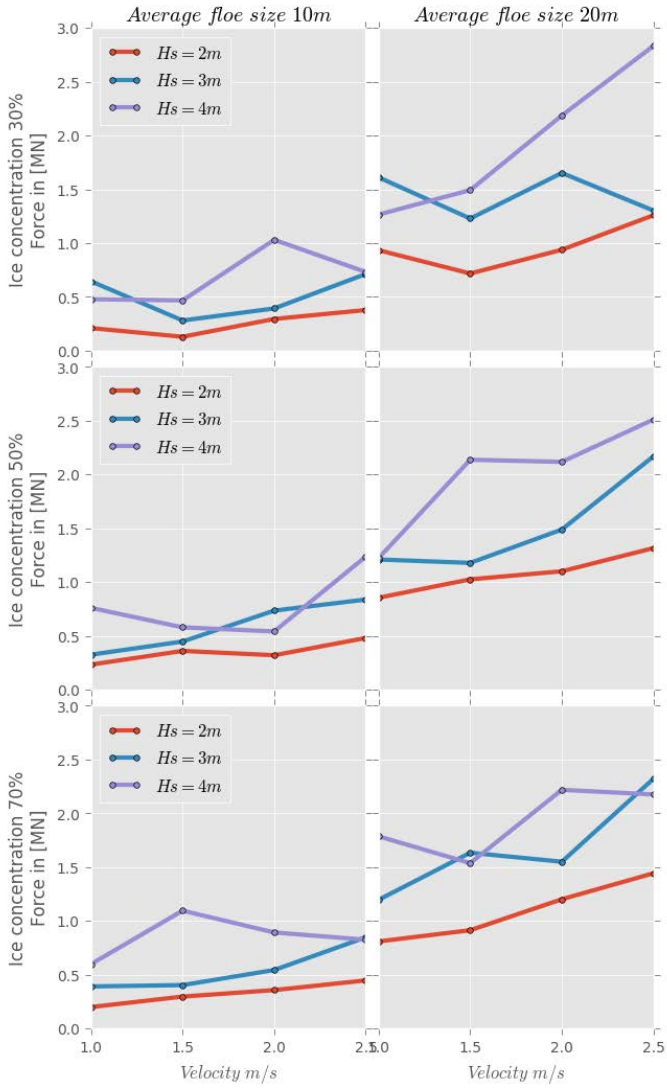

Figure 10. Variation of significant force between vessel speed, significant wave height, floe size and ice concentration.

DISCUSSION

This paper has presented the application of a simplified ice-ice and ice-vessel interaction model together with the inclusion of wave induced forces on both vessel and ice floes. The ice floe model is simplified and the ice floes cannot be broken apart. The significant force of the ice floes shows an increasing tendency when the vessel is moving faster through the ice floe field. This is an expected effect since the impact energies increase. There is

also an increasing tendency for increasing wave height. This effect is in the results in Fig. 10 less visible due to fluctuations in the impact data. It is possible that the distribution of significant wave heights in the simulation setup is too narrow for a meaningful parameter study of the wave effects in the model setup. There are several aspects regarding simulation setups remain for further analysis:

1. The ice floe fields are identical for each concentration and floe size, but are initialized in waves of different length between significant wave height simulations.
2. The ice floes experience forces in opposite directions in the initial phase when distributed over a wave crest.
3. The time from simulation start until the vessel impacts the ice floe field is different depending on vessel speed. This gives slightly different ice floe distributions during traversal of the ice floe field.
4. The impact forces sensitive to blockages and piling of ice floes.

The model nevertheless gives reasonable significant force levels with a marked increase when the floe size increase. Since the model neglects floe failure this is expected, but also a weakness since one can expect more severe interaction forces and possible floe failure with larger floes instead of clearing the floes as with smaller floes. A method to counter the effects of variations of ice floe field is to repeat the scenarios with several floe fields with identical mean size and concertation, but with different distribution of the floes.

The ice accretion has been recorded and while there is a almost linear relationship between floes on the starboard side of the vessel, the vessel hull clears the floes at larger ice concentrations as seen in Fig. 9. From the same figure, it is evident that larger unbreakable floes gives fewer floes in the critical region. This result should be investigated further since it may well be the effect of large unbreakable floes which are cleared by the hull.

CONCLUSION

A simplified ice floe model with wave excitation and hydrodynamic potential damping has been developed and used in a scenario simulation. The significant force calculated by the model seems reasonable but more work is needed to verify the results and remove methodical pitfalls in such parameter variation studies.

ACKNOWLEDGMENTS

This work is financed by the High North Research Centre for Climate and the Environment (Fram Centre, Tromsø, Norway) through the IFISAW (Ice Floe Interaction with Ships and Waves) project.

REFERENCES

[1] Haug, T., Bogstad B., Chierici, M., Gjøsæter, H., Hallfredsson, EH., Høines, ÅS., Hoel, H. 2017. "Future harvest of living resources in the Arctic Ocean north of the Nordic and Barents Seas: A review of possibilities and constraints." Fisheries Research 188 pp. 38-57.

[2] Su, B., Aarsæther, KG., Kristiansen, D.. 2016. "Numerical Study of Wave-Driven Impact of a Sea Ice Floe on a Circular Cylinder." In ASME 2016 35th International Conference on Ocean, Offshore and Arctic Engineering, pp. V008T07A008-V008T07A008. American Society of Mechanical Engineers..

[3] Su, B., Aarsæther, KG., Kristiansen, D., 2017. "Numerical Study of a Moored Structure in Moving Broken Ice Driven by Current and Wave." In ASME 2017 36th International Conference on Ocean, Offshore and Arctic Engineering, pp. V009T12A001-V009T12A001. American Society of Mechanical Engineers.

[4] Løset, S., 1994. "Discrete element modelling of a broken ice field – Part I: model development". Cold Reg. Sci. Technol., 22, pp. 339–347.

[5] Tsarau, A., Løset, S. 2015. "Modelling the hydrodynamic effects associated with station-keeping in broken ice." Cold Regions Science and Technology 118: 76-90.

[6] Tsarau, A., Lubbad R., Løset, S. 2014. "A numerical model for simulation of the hydrodynamic interactions between a marine floater and fragmented sea ice." Cold Regions Science and Technology 103 pp. 1-14.

[7] Lubbad, R., Sveinung Løset, S. 2011. "A numerical model for real-time simulation of ship–ice interaction." Cold Regions Science and Technology 65, no. 2: pp. 111-127.

[8] Metrikin, I., Løset, S. 2013. "Nonsmooth 3d discrete element simulation of a drillship in discontinuous ice." In Proceedings of the International Conference on Port and Ocean Engineering Under Arctic Conditions.

[9] Madsen, NAH., Aarsæther, KG., Herrmann, B., Hansen, K., Jensen, JH. 2016. "The Physical Behavior of Seine Ropes for Evaluating Demersal Seine Fishing." Journal of Offshore Mechanics and Arctic Engineering 138, no. 5.

[10] Reite, KJ, Føre, M., Aarsæther, KG., Jensen, JH., Rundtop, P., Kyllingstad, LT., Endresen, PC., Kristiansen, D., Johansen, V., Fredheim, A.,. 2014. "Fhsim—time domain simulation of marine systems." In ASME 2014 33rd International Conference on Ocean, Offshore and Arctic Engineering, pp. V08AT06A014-V08AT06A014. American Society of Mechanical Engineers.

[11] Fathi, D., and Hoff, JR. 2004. "Shipx vessel responses (veres)." Theory Manual, Marintek AS, Feb 13.

[12] Cummins, W. E., 1962. "The impulse response function and ship motions". No. DTMB-1661. David Taylor Model Basin Washington DC, USA.

[13] Fossen, T. I., 2005. "A nonlinear unified state-space model for ship maneuvering and control in a seaway". International Journal of Bifurcation and Chaos, 15(9), pp. 2717–2746.

[14] WAMIT, Inc., 2013. “WAMIT user manual, Version 7.0”. WAMIT, Inc., Chestnut Hill, MA (2013).

[15] Nezami, E.G., Hashash, Y.M.A., Zhao, D. and Ghaboussi, J., 2004. "A fast contact detection algorithm for 3-D discrete element method". Comput. Geotech., 31, pp. 575–587.

[16] Cundall, P.A., 1988. "Formulation of a three-dimensional distinct element model-part I: a scheme to detect and represent contacts in a system composed of many polyhedral blocks". Int. J. Rock Mech. Min. Sci. & Geomech. Abstr., 25(3), pp.107–116.

[17] Faltinsen, O., 1993. Sea loads on ships and offshore structures. Cambridge university press.

[18] Newman, J. N., 1977. Marine hydrodynamics. MIT press.

[19] Fossen, T. I., 2011. Handbook of Marine Craft Hydrodynamics and Motion Control. Wiley & Sons